 doi:10.20944/preprints202202.0037.v1

Article

Investigation of elastic properties of WO_3 thin films supported on Quartz in SAW sensing devices

Madjid Arab*, Véronique Madigou, Virginie Chevallier, Christian Turquat, Christine Leroux

Aix Marseille Univ, Université de Toulon, CNRS, IM2NP, Marseille France, CS 60584, Toulon Cedex 9, F-83041, France

* Correspondence: madjid.arab@univ-tln.fr; Tel.: (+33) 494 142 533

Abstract: This study aimed to discuss the combined theoretical and experimental results of elastic properties of the tungsten trioxide films supported on Quartz (YX)/45°/10° resonator, as surface acoustic wave (SAW) device. The SAW system with different thicknesses of WO_3 thin films were imaged and structurally characterized by X-Ray diffraction, atomic force and transmission electron microscopy. The deposited WO_3 films (100 nm, 200 nm and 300 nm) were crystallized in a single monoclinic phase. The acoustoelectric properties of the SAW system were obtained by combining theoretical simulations with experimental measurements. The modeling of the SAW devices has been performed by the finite element and boundary element methods (FEM/BEM). The theoretical and experimental electrical admittances responses obtained at room temperature gave access to elastic constants. The gravimetric effect of the deposited layers is observed by a resonance frequencies shift to lower values with thicknesses film. Moreover, the acoustic losses are affected by the dielectric losses of the WO_3 films, while the resonant frequency decreases almost linearly. SAW devices revealed strong displacement fields with low acoustic losses as a function of WO_3 thicknesses. For all the deposited layers, the Young's modulus and the Poisson coefficient obtained are respectively of 8 GPa and 0.5.

Keywords: SAW devices, Tungsten trioxide, FEM/BEM, Harmonic admittance, elastic properties

1. Introduction

Surface acoustic wave (SAW) devices have been largely studied as chemical gas. They are very attractive because of their high sensitivity due to modification of the propagating wave, introduced by the interaction of the active material with specific gas molecules [1],[2],[3],[4]. This results from the wave energy that is confined near the piezoelectric crystal surface within few wavelengths [5]. Consequently, the surface wave resonator is strongly sensitive to any changes of the physical and/or chemical properties of the thin active layer (as in our case). As long as the thickness of the sensitive material is less than the wavelength of the surface wave, these can be considered Rayleigh waves. The associated mechanisms (phenomena) are mass loading effects, changes of the elastic properties and electrical conductivity [6],[7],[8].

The electrical conduction variations of the sensitive film disturb the propagation of the acoustic wave on the quartz surface and consequently its acoustic speed. The first study on the acoustoelectric effects was demonstrated on SAW sensor covered with a semiconductor thin film under hydrogen exposure [9]. This effect is generalized through an acoustoelectric parameter calculation showing that the wave propagation is affected either by mass effect, change in electrical conductivity of the film, or by combining both [10],[11].

The tungsten trioxide WO_3 is a well known material in sensor technology that has been studied extensively, particularly by our lab [12],[13]. Moreover, WO_3 based materials as heavy metal oxide have been considered as promising glasses materials due to their high thermal stability, good mechanical properties and electrical conductivity [14],[15].

Preprints (www.preprints.org) | NOT PEER-REVIEWED | Posted: 2 February 2022 doi:10.20944/preprints202202.0037.v1

Ideally, the tungsten trioxide structure is cubic and formed by three-dimensional network of corner sharing of the octahedra [16]. However, the structure of WO_3 reveals phase transitions as a function of the preparation temperature, showing a polymorphic behavior. This corresponds to the distortion of the network, tilting of the octahedra or ions displacement (and/or induced vacancies) leading to different crystallographic structures. Thus, all modifications of WO_3 crystal network depend on the various oxidation states of the different coordination polyhedral [17].

Currently, the elastic parameters of WO_3 in single crystal or powder form have been determined using atomic level simulation methods [18]. However, to date, no simple and reproducible method has been able to determine the elastic constants of materials in the thin layer form. In other words, the acoustic characterization of WO_3 as thin films is almost non-existent in the literature. Thus, we considered the elastic constants found in the literature as a starting point for the fitting of the elastic parameters.

Our theoretical study offers a methodology, which allows starting from unknown physical parameters of an element constituting the acoustic component and from agreement simulation-measurement agreement, to estimate the elastic parameters of the thin film deposited on the SAW resonator. The modeling of the SAW devices has been performed by the finite element method (FEM). It is based on the adjustment of the thin layer density allowing the agreement between simulations and measurements. This work deals with the direct analysis of the acoustoelectric signals of different layers deposited on SAW resonator to extract some physical properties of the material such as the Young's modulus E, the Poisson's ratio ν. The originality of this work lies in the use of SAW devices to study the electromechanical behavior of thin layers constituting our SAW sensor.

2. Experimental and theoretical approach

2.1. *SAW sensing device*

SAW device configuration: SAW device consists in a Quartz (YX)/45°/10° resonator equipped with a transducer and IDTs interdigital structures used as reflectors and different layers of WO_3. The surface wave devices that were used to perform this study are quartz-based single-port resonators operating at 434 MHz. Figure 1 represents the typical structure of the SAW transducer used. Table 1 groups the physical characteristics of SAW devices.

In all cases, the layer deposited on the piezoelectric substrate acts as a sensitive layer but also as a guide for the elastic waves; this is done by judiciously choosing the possible vibration modes of the structure and the anisotropy properties of the considered substrates.

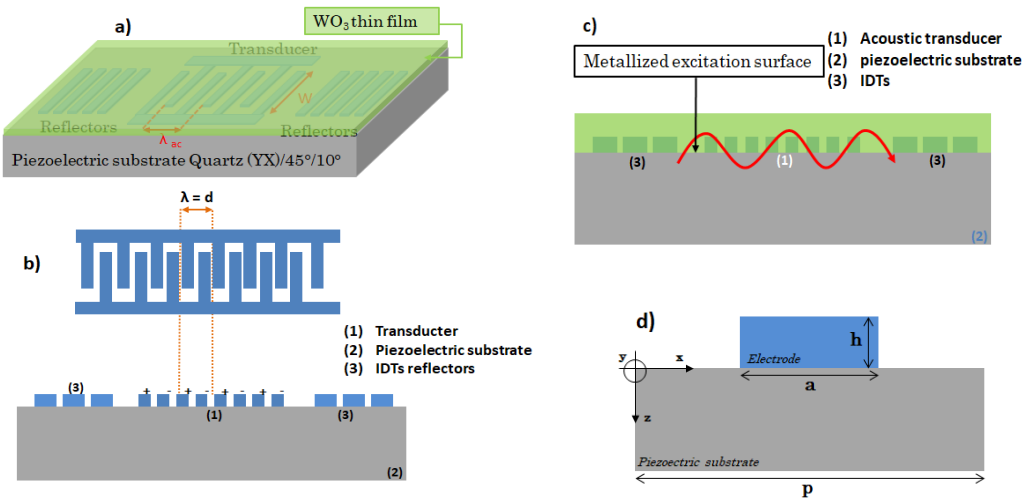

Preprints (www.preprints.org) | NOT PEER-REVIEWED | Posted: 2 February 2022 doi:10.20944/preprints202202.0037.v1

Figure 1. a) Schematic of SAW device with a WO_3-coated quartz, b) configuration of the IDTs transducer, c) SAW system with metallized excitation surface and d) Representation of an elementary cell.

The WO_3 layers were deposited on the entire surface of the resonator, as shown in figure 1. The interest of such configuration is to work with waves propagating on the metallized excitation surface and not on the free surface (figure 1.c). The interest is to significantly improve the sensitivity to the effects of films conductivity variation.

2.2. *Experimental setup*

Film synthesis: WO_3 films were prepared by reactive radio frequency (13.56 MHz) magnetron sputtering, using a 99.9% pure tungsten target. The thin films were sputtered on quartz substrate of SAW devices with aluminum electrodes, in a reactive atmosphere under oxygen–argon mixture ($P_{Ar}/P_{(O2)}$ =1.6). Several WO_3 layers with different thicknesses, have been deposited. After layer deposition, the films were annealed at 400°C for 3 hours in air in order to stabilize the chemical composition and the crystalline structure. The synthesis setup and standard procedure have been already published with more details [12],[13].

Characterization methods: The morphological analyses of WO_3 thin films were conducted by Atomic Force microscopy (AFM) and with a conventional Transmission Microscope (TEM), Tecnai 200 kV, equipped with a LaB6 source.

The structural characterization of WO_3 films were obtained by X-ray powder diffraction (XRD) in the classical θ-2θ mode, from 10° to 80◎ (step size 0.003°, scan speed 0.004°s-1), with an Empyrean Panalytical diffractometer, equipped with a Cu anticathode. X-ray patterns were compared with those of the Inorganic Crystal Structure datasheets (ICSD).

Acoustic measurement: The output signal of SAW devices was measured by a HP Agilent 4396B network analyser. The set parameters of (YX)/45°/10° quartz SAW resonator are reported in table 1.

Table 1. The IDT specifications of YX/45°/10° quartz SAW resonator

Resonator type	Quartz *(YX/45°/10°)*
Type of electrodes	Aluminium
Electrode width *a* (μm)	2,9
IDT period *p* (μm)	3,63
Wavelegnth λ (μm)	8
Electrode thickness *h* (nm)	120
Metallization ratio *a/p*	0,8
Metallization thickness *h/* λ *(%)*	1,5
Acoustic velocity *v* (m/s)	3462

2.3. *Simulation*

For theoretical acoustic studies, we used a combination of finite element and boundary element methods (FEM/BEM), widely used to model complex multilayer systems, such as SAW device[19],[20],[21],[22]. To simulate our piezoelectric resonators, we have built a model that takes into account each material constituting the SAW devices. This approach is similar to the one conducted with volume wave acoustic resonators [23]. Each element can be considered as points of a given structure for which the physical parameters will be computed using the finite element method coupled with that of boundary elements. Each subset constitutes a domain, which makes the structure discontinuous. However, in order to give the best account of the physical quantities of our system, it must be seen as a set of

Preprints (www.preprints.org) | NOT PEER-REVIEWED | Posted: 2 February 2022 doi:10.20944/preprints202202.0037.v1

continuous domains, hence the need to discretize the volume or the study surface by creating a mesh. The mesh, represented in figure 2, subdivides the study area into sub-elements or finite elements, interconnected by particular points called "nodes".

The propagation of acoustic waves in linear homogeneous media can be formulated as an eigenvalue problem according to the Fahmy-Adler approach [24]. We consider that the propagation in the (x,z) plane and the dependence along y is given by the system to solve. We define a state vector mixing displacements and generalized constraints in the propagation plane and implicitly the time dependence is harmonic type ($e^{j\omega t}$).

The calculation is based on the stress relations (Hooke's law extended to piezoelectricity) and the electric displacement vector to define an eigenvalue system [25],[26].

$$T_i = C_{ijkl}\, S_{kl} + e_{ijk} E_k \quad (1)$$

$$D_i = e_{ikl}\, S_{kl} - e_{ik} E_k \quad (2)$$

where T is the stress tensor, C is the elastic stiffness tensor, S is the elastic strain tensor, e is the piezoelectricity tensor, E is the electric field, D is the electric displacement, ε is the dielectric permittivity tensor and *i* represents the three direction (x, y, z).

The usual piezoelectric coefficient *e* is expressed in matrix form as follows: $e = d.C$, where [C] is the elastic stiffness matrix and [d] is the piezoelectric strain coefficient matrix of quartz. In the case of anisotropic materials, the existence of symmetries in a crystal reduces the number of admissible stiffness tensor components C_{ijkl} (independent elastic constants) to 21. Given the trigonal symmetry, α-quartz has 6 independent elastic constants.

The isotropic character of a cubic structure, as it is the case of tungsten oxide WO_3 (see structural characterization section), satisfies the relation: $2C_{66} = C_{11}\text{-}C_{12}$. The Young's modulus (E) and the Poisson's ratio (ν) are then expressed in terms of the elastic constants C_{11}, C_{12} and C_{66} as follows :

$$\nu = \frac{C_{12}}{C_{11}} \quad (3)$$

$$E = \frac{4\, C_{66}(C_{11} - C_{66})}{C_{11}} \quad (4)$$

To characterize the propagation of acoustic waves generated by the piezoelectric effect, conditions on the boundaries of the resolution domain are associated with the constitutive equations of piezoelectricity. The piezoelectric material should not be treated as an infinite substrate, but with dimensions defined by mechanical and electrical boundary conditions.

- For the electrical domain, a potential difference is assigned to the electrodes
- The mechanical stress T is zero at the free surfaces of WO_3 and the electrodes.
- The boundary conditions at the piezoelectric substrate-electrode and piezoelectric substrate-WO_3 interfaces require continuous mechanical displacements and stresses.

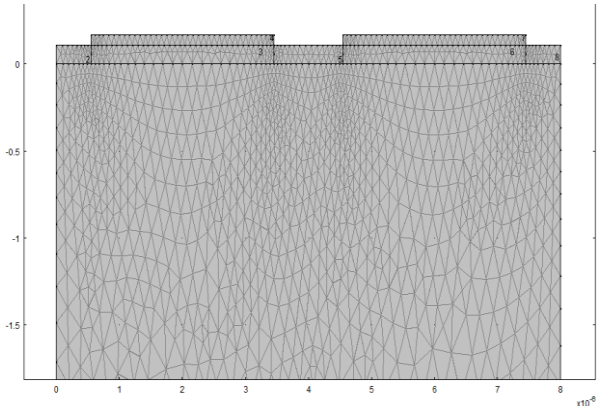

Preprints (www.preprints.org) | NOT PEER-REVIEWED | Posted: 2 February 2022 doi:10.20944/preprints202202.0037.v1

Figure 2. Representation of the typical mesh of two neighboring electrodes of a periodic array covered with WO_3 films.

3. Results and discussion

3.1. Structural and morphological characterization of WO_3 thin films

Figure 3a represents the typical X-Ray diffraction patterns of WO_3 films with thicknesses of 100 nm, 200nm and 300nm. The identified diffraction Bragg peaks are characteristic of a single-phase monoclinic structure of WO_3 according to the ICSD standard database (ICSD datasheet N° 050727). As reported in a previous study, the experimental XRD patterns and Rietveld refinement are in good agreement, such as the broad peaks indicates small crystallites around 40nm (± 10nm). The monoclinic phase is a distorted ReO_3 cubic phase based on tridimensional networks of corners – sharing WO_6 octahedra. The three films have similar structure based on tridimensional networks of corners – sharing WO_6 octahedra.

The tilt and the distortion of the octahedra, lead to monoclinic phase whereas ideal ReO_3 structure (without tilting) corresponds to the cubic structure. We observed that intensity of the (200) and (020) peaks decreases while that of the (002) peak increases, with the increase of film thickness corresponding to the modification of the film orientation with thickness. According to structural results, all WO_3 films have similar structure close to the cubic phase that behave as an isotropic system. As a function of the thicknesses deposited, the three main peaks oriented in the main directions change in intensity and width at mid-height. The lattice parameters show a little variation and remain close to the cubic phase for all films, resulting in the set of values: a = 7.316 Å, b= 7.528 Å, c = 7.397 Å, $\alpha = \gamma = 90°$ and $\beta = 90.82°$ that are associated to the space group of $P12_1/C$.

The TEM image (figure 3b) is an example of cross section of a WO_3 film deposited on quartz substrate, the measured thickness is 200 nm. The electronic diffraction pattern of a selected area (insert figure 3b) shows that the film is monocrystalline and confirms the distorted cubic phase, in agreement with XRD results: the strong spot correspond to the initial cubic phase and the weak ones are induced by the deformation of the octahedral.

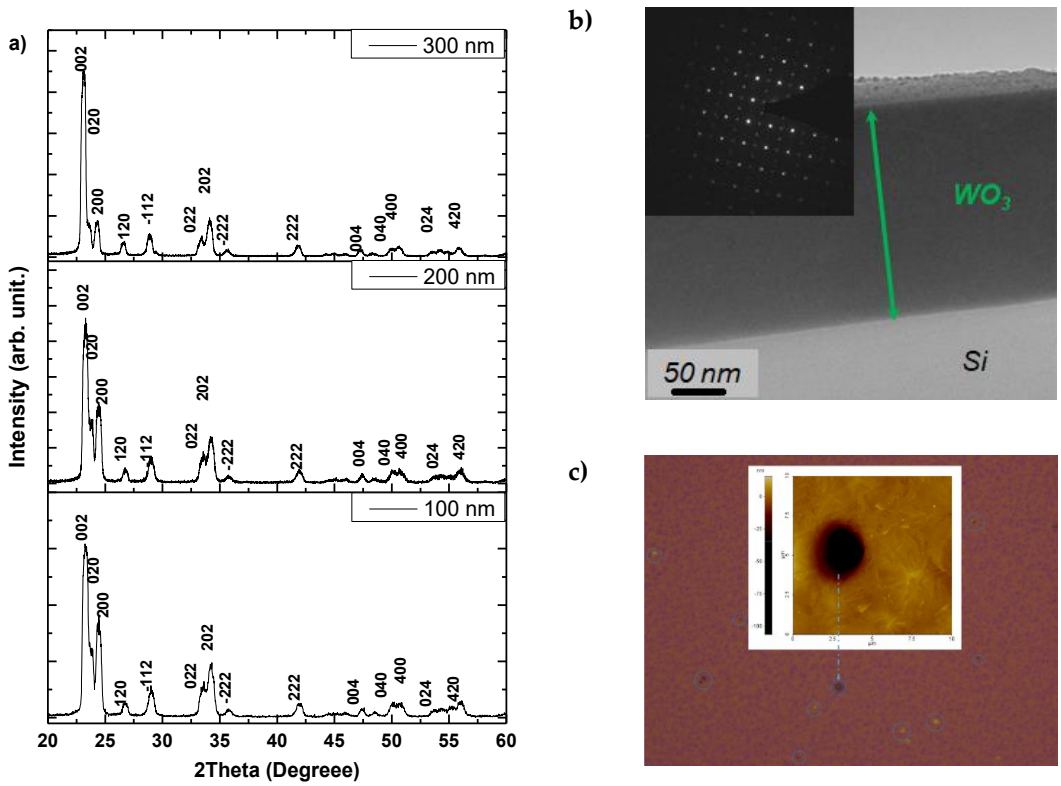

Preprints (www.preprints.org) | NOT PEER-REVIEWED | Posted: 2 February 2022 doi:10.20944/preprints202202.0037.v1

Figure 3. a) XRD pattern of the deposited WO_3 films, b) TEM cross section of 200 nm thick film, the insert picture correspond to the electronic diffraction pattern, c) AFM image of the surface of a film on SAW.

The AFM images (as an example the figure 3c) of the deposited films reveals the a weak roughness and a high porosity. This porosity increases with the film thickness from 100 nm to a few microns. Moreover, this analysis allowed us to verify the thickness of the deposited layers by using the largest pores.

3.2. Piezoelectric characteristic

To model the electromechanical behavior of surface acoustic wave devices, the periodic electrode array must be decomposed into elementary single-electrode cells to evaluate the impact of electrical behavior on wave propagation (Figure 1.d). From theoretical calculations, it is possible to determine the harmonic admittance. This method was developed by Ventura [27] and then by Baghaï-Wadji [28].

3.2.1. *Sensitivity to the gravimetric effect*

First, we investigated the gravimetric sensitivity of these acoustic systems when they are coated with a thin layer of tungsten oxide 100 nm, 200 nm and 300 nm thick. To do this, we have calibrated the simulation calculations on the experimental results performed at 25°C. We assumed that the WO_3 thin films were homogeneous and uniformly distributed on the whole resonator, i.e. on the reflectors and the transducer. We also assumed that the material covered the acoustic component by reproducing the initial relief induced by the presence of the electrodes.

To evaluate the gravimetric influence on the acousto-electric signal response due to the presence of metal oxide WO_3, we considered the case of a metallized surface excited wave with free charge motion modeled by Green function (figure 1.c). The harmonic admittance is given by the evolution of the conductance and the harmonic susceptance as a function of the frequency, defined by Y(f)= G(f)+j B(f). Figure 4 shows the measured admittances on resonators for three different thicknesses of WO_3 thin film. After integration of WO_3 with different thicknesses (passivation effect), we observed a significant shift towards low frequencies highlighting the mass effect following the deposition. As known, the masse – frequency shift variation is described by the Sauebrey relation as : $\Delta f = -\frac{2f_0^2}{\sqrt{C_{66}\rho_q}}\Delta m$ (f_0 is SAW resonance frequency and ρ_q is quartz density). To take into account the passivation effect, we had to consider frequency shifts of 18, 26 and 45 MHz respectively for thicknesses of 100, 200 and 300 nm. We observe the disappearance of the exploitable resonance conditions for a film of 300 nm thick. Therefore, this thickness value is considered as the maximum thickness compatible with proper use of the acousto-electric signals from Rayleigh wave resonators.

Preprints (www.preprints.org) | NOT PEER-REVIEWED | Posted: 2 February 2022 doi:10.20944/preprints202202.0037.v1

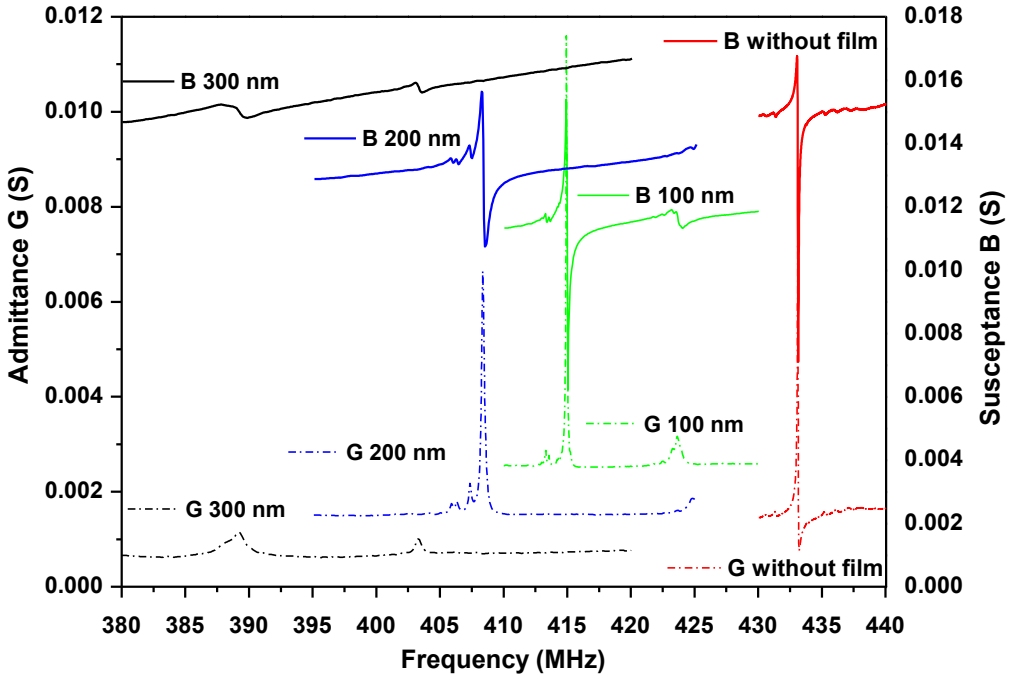

Figure 4. Experimental admittances of Quartz (YX)/45°/10° alone and with WO_3 films, 200 nm et 300 nm.

3.2.2. *Sensitivity to the variations of the WO_3 films dielectric properties*

To consider the impact of conduction effects in the WO_3 semiconductor layer on the acoustic wave properties, free charges must be introduced. The sensitivity of the surface acoustic wave propagation parameters to the effects of variations in the dielectric properties of the metal oxide layer is monitored by the dielectric losses, denoted tan(δ) such that:

$$tan(\delta) = \frac{\sigma}{\varepsilon\,\omega} \tag{5}$$

where σ is the real conductivity, ε the dielectric permittivity and ω is the pulsation. For all simulations, a dielectric constant of 5.24 was set as reported in the literature [29].
Considering the WO_3 film being of cubic structure and conducting behavior, the displacement of free charges under the action of an electric field (E) is described by the following equation [30]:

$$\sigma_{ij}\frac{\partial E_j}{\partial x_i} + jw\varepsilon_{ij}\frac{\partial E_j}{\partial x_i} = 0 \tag{6}$$

Some of the electroacoustic energy is converted to conduction current in the sensitive layer, resulting in attenuation of the wave as it propagates. These losses will be all the more important as the electromechanical coupling is strong.
The simulation of the acoustic losses of the resonator according to the dielectric characteristics of the sensitive layer of WO_3 was carried out with devices covered with 100 nm and 200 nm thickness. The parameters thus determined were deduced from Green's function calculations which allow to characterize the sensitivity of the wave properties (phase velocity, acoustic losses and electromechanical coupling) at first order.
Figures 5, show the acoustic losses as a function of the dielectric losses around the resonant frequency for each film thickness. It can be seen that the acoustic losses are slightly affected by the dielectric losses of the WO_3 films. At the same time, the frequency decreases almost linearly. The acoustic losses increase with the thickness of the deposited films, to the limit of 300 nm.

Preprints (www.preprints.org) | NOT PEER-REVIEWED | Posted: 2 February 2022 doi:10.20944/preprints202202.0037.v1

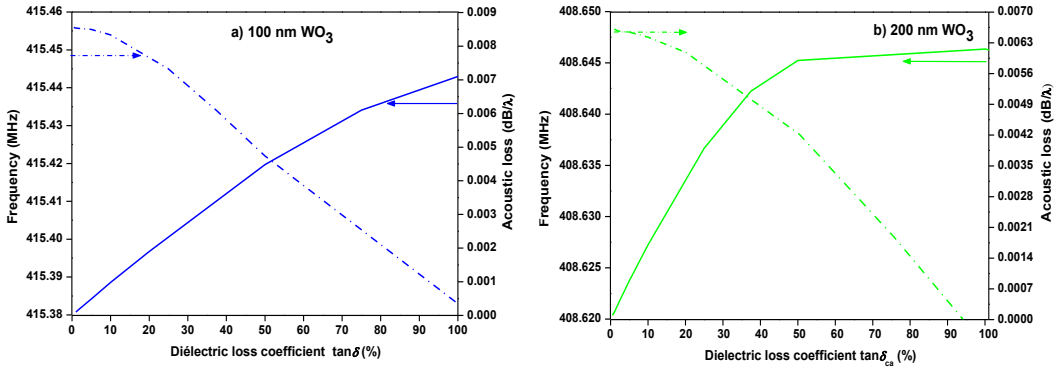

Figure 5. Evolution of acoustic and dielectric losses and frequencies for a resonator covered with a WO_3 film of thickness : a) 100 nm and b) 200 nm.

3.2.3. *Elastic properties of WO_3 thin films*

It is important to point out the lack of data about the elastic properties of WO_3 as a thin film. Therefore, we considered the elastic constants found in the literature as a starting point for fitting the elastic parameters. To simplify the simulation calculations, we assumed that the sensitive layer is isotropic. Figure 6 represents the theoretical and experimental electroacoustic responses (electrical admittances) obtained at room temperature in the case of quartz resonators (YX)/45°/10°. The signals obtained show the presence of a clear resonance at the end of the stop band corresponding to a precise reflection coefficient. This characteristic allowed us to determine the properties of the WO_3 layer. For each configuration, a set of constants was adjusted to obtain maximum agreement between the simulated and experimental results, reported in Table 2. As can be seen, the acoustic dissipation increases as a function of WO_3 thickness such that above 300nm, the experimental signal was no longer usable (Figure 6). In addition, the viscoelastic losses of the overlay were also adjusted according to the experimental observations, resulting in an equivalent mechanical quality factor of 50.

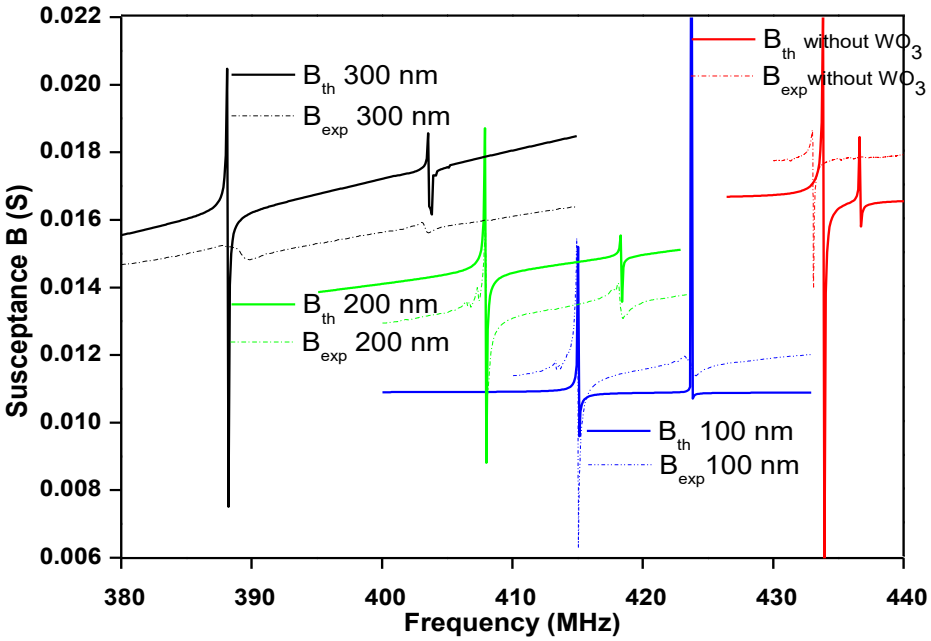

Figure 6. Theoretical and experimental responses of quartz (YX)/45°/10° resonators for different WO_3 thicknesses : 100 nm, 200 nm and 300 nm.

As shown in Table 2, the density was varied for each WO_3 thickness to obtain the best fits. The obtained results with SAW resonator, show similar elastic characteristic than those

Preprints (www.preprints.org) | NOT PEER-REVIEWED | Posted: 2 February 2022 doi:10.20944/preprints202202.0037.v1

obtained with bulk acoustic wave (BAW) resonator. SAW results are slightly lower but remain of the same order of magnitude as those obtained using BAW [23]. This agreement shows that our approach remains reliable for the evaluation of elastic constants.
One can imagine the mass density unchanged with respect to the thickness of WO_3 film, but the ratio between the elastic constants would then have remained unchanged. From a technological point of view, the film is polycrystalline and the porosity size is affected by the thickness of the deposited layers. Within each grain, the elasticity behavior is not modified but the total mass of the layer does increase as a function of the deposit (thickness).

Table 2. Elastic constants of WO_3 thin film at 100 nm, 200 nm and 300 nm thicknesses obtained from modeling of quartz (YX)/45°/10° resonators by the mixed matrix method.

Resonator	Quartz (YX)/45°/10°		
Thickness of WO_3	100 nm	200 nm	300 nm
Density ϱ (kg/m³)	6500	4700	3900
C_{11} (GPa)	14	15	12,5
C_{12} (GPa)	8	8	7
C_{66} (GPa)	2,5	2,5	2,5
Poisson Coefficient ν	0,57	0,53	0,56
Young's modulus E (GPa)	8,2	8,3	8.0

To explain the low values of elastic constants found in table 2 compared to those obtained in the literature [18], we made the assumption that it is mainly the grains boundary of WO_3 that respond to the acoustic disturbance. We therefore considered WO_3 as a two-dimensional plate consisting of grains and grain boundaries. Under the external stress action, the elastic deformation within the material occurs at the grain boundaries. In this case, the elastic constants C*ij* define the local deformation leading to an electroacoustic response of the device.
The simulations were performed at different levels to differentiate the eigenmodes from the parasitic modes and to calculate the resonance frequency of our systems constituted by the piezoelectric substrate and the electrodes in presence or not of a WO_3 layer. The maps shown on figure 7 give the thickness shearing vibration mode (TSM) representing the displacement fields in a SAW system.

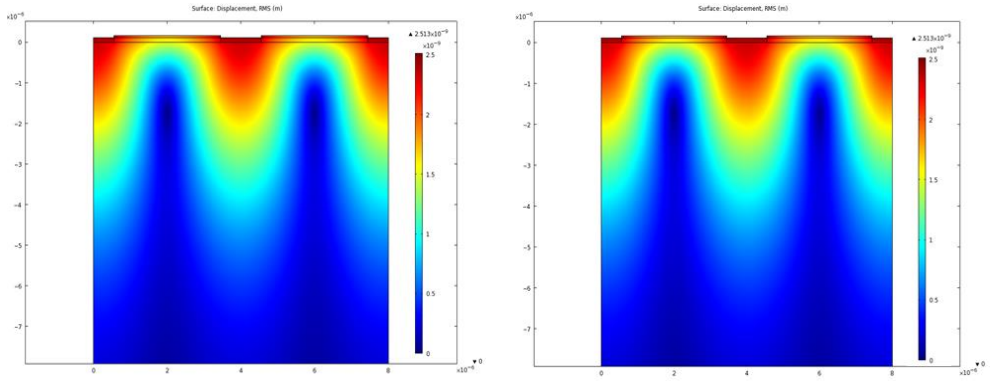

Without films 100 nm of WO_3

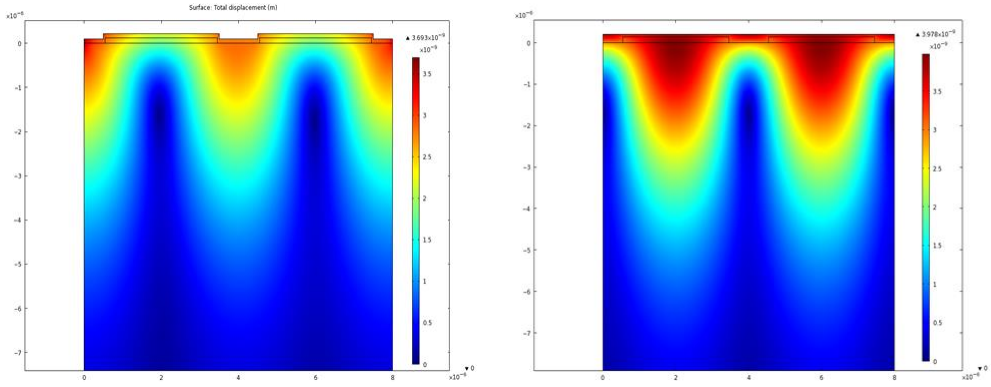

200 nm of WO_3 300 nm of WO_3

Figure 7. Displacement modes in SAW devices for different layers.

4. Conclusions

The elastic properties of tungsten trioxide films were investigated in SAW sensor devices. The deposited layers, 100 nm to 300 nm, crystallized in a single-phase monoclinic structure, obtained after calcination at 400°C. The analysis of the surface showed the presence of a strong porosity, ranging from a hundred nanometers to a few micrometers. Consequently, the effective volume densities decrease with the thickness of the WO_3 layers.
The harmonic admittance obtained by simulations using FEM/BEM methods combined with experimental measurements allowed to evaluate the effective elastic constants Cij of WO_3 films. The calculated Young's modulus and Poisson's coefficient are respectively of the order of 8 GPa and 0.5. The electroacoustic modeling of SAW gives us information on the elastic deformation not of the completely thin layer but rather at the local level, at the interface between the grain boundaries constituting the crystal.
The SAW electroacoustic responses to the gravimetric effect and acoustic loss are sensitive to the thickness of the deposited layers. As the thickness increases, resonance frequency shifts to lower values and are followed by acoustic losses. Moreover, the displacement fields linked to the deformations become very important at the interface electrode - WO_3 films.

Author Contributions: Conceptualization, methodology, and investigation, M. A; formal analysis and data curation, V. M., V. C., Ch. L.; writing—original draft preparation, M. A.; writing—review and editing, M. A., V. M., V. C., Ch. L.; supervision, project administration, and funding acquisition, M. A.; All authors have read and agreed to the published version of the manuscript..

Funding: We gratefully acknowledge the Regional Council of Provence-Alpes-Côte d'Azur General Council of Var, the agglomeration community of Toulon Provence Mediterranean and Toulon University for their financial supports in the framework of the "Nanomaterials for sensor devices" project..

Institutional Review Board Statement: Not applicable.

Informed Consent Statement: Not applicable.

Data Availability Statement: The data presented in this study are available on request from the corresponding author.

Conflicts of Interest: The authors declare no conflict of interest.

References

1. Pan, Y., Molin, Q., Guo, T., Zhang, L., Cao, B., Yang, J., … Xue, X. (2021). Wireless passive surface acoustic wave (SAW) technology in gas sensing. Sensor Review, 41(2), 135–143. https://doi.org/10.1108/SR-03-2020-0061
2. Palla-Papavlu, A., Voicu, S. I., & Dinescu, M. (2021). Sensitive Materials and Coating Technologies for Surface Acoustic Wave Sensors. Chemosensors, 9(5), 105. https://doi.org/10.3390/chemosensors9050105

3. David, M., Arab, M., Martino, C., Delmas, L., Guinneton, F., & Gavarri, J.-R. (2012). Carbon nanotubes/ceria composite layers deposited on surface acoustic wave devices for gas detection at room temperature. Thin Solid Films, 520(14), 4786–4791. https://doi.org/10.1016/j.tsf.2011.10.166
4. Devkota, J., Ohodnicki, P., & Greve, D. (2017). SAW Sensors for Chemical Vapors and Gases. Sensors, 17(4), 801. https://doi.org/10.3390/s17040801
5. Briscoe, J. (2014). Nanostructured piezoelectric energy harvesters. New York: Springer.
6. Mauder, A. (1995). SAW gas sensors: comparison between delay line and two port resonator. Sensors and Actuators B: Chemical, 26(1–3), 187–190. https://doi.org/10.1016/0925-4005(94)01583-4
7. Anisimkin, V. I., Kotelyanskii, I. M., Fedosov, V. I., Caliendo, C., Verardi, P., & Verona, E. (1995). Analysis of the different contributions to the response of SAW gas sensors. In 1995 IEEE Ultrasonics Symposium. Proceedings. An International Symposium (Vol. 1, pp. 515–518). Presented at the 1995 IEEE Ultrasonics Symposium. An International Symposium, Seattle, WA, USA: IEEE. https://doi.org/10.1109/ULTSYM.1995.495630
8. Ricco, A. J., & Martin, S. J. (1991). Thin metal film characterization and chemical sensors: monitoring electronic conductivity, mass loading and mechanical properties with surface acoustic wave devices. Thin Solid Films, 206(1–2), 94–101. https://doi.org/10.1016/0040-6090(91)90399-I
9. Jakubik, W. P. (2011). Surface acoustic wave-based gas sensors. Thin Solid Films, 520(3), 986–993. https://doi.org/10.1016/j.tsf.2011.04.174
10. Ippolito, S. J., Kandasamy, S., Kalantar-Zadeh, K., & Wlodarski, W. (2005). Layered SAW hydrogen sensor with modified tungsten trioxide selective layer. Sensors and Actuators B: Chemical, 108(1–2), 553–557. https://doi.org/10.1016/j.snb.2004.11.048
11. Sadek, A. Z., Wlodarski, W., Shin, K., Kaner, R. B., & Kalantar-zadeh, K. (2008). A polyaniline/WO_3 nanofiber composite-based ZnO/64° YX $LiNbO_3$ SAW hydrogen gas sensor. Synthetic Metals, 158(1–2), 29–32. https://doi.org/10.1016/j.synthmet.2007.11.008
12. Guérin, J., Bendahan, M., & Aguir, K. (2008). A dynamic response model for the WO3-based ozone sensors. Sensors and Actuators B: Chemical, 128, 462–467. https://doi.org/10.1016/j.snb.2007.07.010
13. Faleh, R., Gomri, S., Aguir, K., & Kachouri, A. (2021). A new combined transient extraction method coupled with WO_3 gas sensors for polluting gases classification. Sensor Review, 41(5), 437–448. https://doi.org/10.1108/SR-02-2021-0066
14. Ovcharenko, N. V., & Smirnova, T. V. (2001). High refractive index and magneto–optical glasses in the systems TeO_2–WO_3–Bi_2O_3 and TeO_2–WO_3–PbO. Journal of Non-Crystalline Solids, 291(1–2), 121–126. https://doi.org/10.1016/S0022-3093(01)00793-1
15. Mahmoud, I. S., Issa, Shams. A. M., Zakaly, H. M. H., Saudi, H. A., Ali, A. S., Saddeek, Y. B., … Tekin, H. O. (2021). Material characterization of WO_3/$Bi2O_3$ substituted calcium-borosilicate glasses: Structural, physical, mechanical properties and gamma-ray resistance competencies. Journal of Alloys and Compounds, 888, 161419. https://doi.org/10.1016/j.jallcom.2021.161419
16. Dirany, N., Arab, M., Madigou, V., Leroux, Ch., & Gavarri, J. R. (2016). A facile one step route to synthesize WO_3 nanoplatelets for CO oxidation and photodegradation of RhB: microstructural, optical and electrical studies. RSC Advances, 6(73), 69615–69626. https://doi.org/10.1039/C6RA13500E
17. Chatten, R., Chadwick, A. V., Rougier, A., & Lindan, P. J. D. (2005). The Oxygen Vacancy in Crystal Phases of WO_3. The Journal of Physical Chemistry B, 109(8), 3146–3156. https://doi.org/10.1021/jp045655r
18. Dendzik, z., Dhrobak, d., & Nowak, r. (2009). Nlastic constants and analytic bond order potential for atomistic simulations of simple cubic tungsten trioxide. Task Quarterly, pp. 93–98.
19. Ventura, P., & Steichen, W. (2007). FEM/BEM Analysis of a Generalized Periodic Array. IEEE Transactions on Ultrasonics, Ferroelectrics, and Frequency Control, 54(10), 2052–2059. https://doi.org/10.1109/TUFFC.2007.500
20. Perois, X., Pastureaud, T., Girard, P.-A., & Lardat, R. (2005). Analysis of saw devices using FEM/BEM method and parallel computing. In IEEE Ultrasonics Symposium, 2005. (Vol. 3, pp. 1564–1567). Presented at the IEEE Ultrasonics Symposium, 2005., Rotterdam, The Netherlands: IEEE. https://doi.org/10.1109/ULTSYM.2005.1603158
21. Ventura, P., & Gratier, J. (2008). FEM/BEM analysis of infinite periodic grating covered with an SiO_2 overlay. In 2008 IEEE Ultrasonics Symposium (pp. 815–819). Presented at the 2008 IEEE Ultrasonics Symposium (IUS), Beijing, China: IEEE. https://doi.org/10.1109/ULTSYM.2008.0196
22. Li, H., Lu, Z., Ke, Y., Tian, Y., & Luo, W. (2019). A Fast Optimization Algorithm of FEM/BEM Simulation for Periodic Surface Acoustic Wave Structures. Information, 10(3), 90. https://doi.org/10.3390/info10030090
23. Arab, M., Dirany, N., & David, M. (2016). BAW Resonator as Elastic Characterization Tools of WO3 Thin Films. Materials Today: Proceedings, 3(2), 152–156. https://doi.org/10.1016/j.matpr.2016.01.047
24. Fahmy, A. H., & Adler, E. L. (1973). Propagation of acoustic surface waves in multilayers: A matrix description. Applied Physics Letters, 22(10), 495–497. https://doi.org/10.1063/1.1654482
25. Chopra, I. (2002). Review of State of Art of Smart Structures and Integrated Systems. AIAA Journal, 40(11), 2145–2187. https://doi.org/10.2514/2.1561
26. Covaci, C., & Gontean, A. (2020). Piezoelectric Energy Harvesting Solutions: A Review. Sensors, 20(12), 3512. https://doi.org/10.3390/s20123512

 doi:10.20944/preprints202202.0037.v1

27. Ventura, P., Dufilie, P., & Hecht, F. (2014). Full analysis of the mixed matrix parameters for a SAW transducer having aperiodic multi electrode cells. In 2014 IEEE International Ultrasonics Symposium (pp. 1492–1496). Presented at the 2014 IEEE International Ultrasonics Symposium (IUS), Chicago, IL, USA: IEEE. https://doi.org/10.1109/ULTSYM.2014.0369
28. Reichinger, H. P., & Baghai-Wadji, A. R. (1992). Dynamic 2D analysis of SAW-devices including massloading. In IEEE 1992 Ultrasonics Symposium Proceedings (pp. 7–10). Presented at the IEEE 1992 Ultrasonics Symposium Proceedings, Tucson, AZ, USA: IEEE. https://doi.org/10.1109/ULTSYM.1992.276073
29. Salje, E. (1975). Lattice dynamics of WO_3. Acta Crystallographica Section A, 31(3), 360–363. https://doi.org/10.1107/S0567739475000757
30. Royer, D., & Dieulesaint, E. (1996). Ondes élastiques dans les solides. Paris Milan Barcelone: Masson.
31. Lu, F., Lee, H. P., & Lim, S. P. (2004). Quartz crystal microbalance with rigid mass partially attached on electrode surfaces. Sensors and Actuators A: Physical, 112(2–3), 203–210. https://doi.org/10.1016/j.sna.2004.01.018